

Lyman continuum leaking AGN in the SSA22 field*

Genoveva Micheva,¹ Ikuru Iwata,^{1,2} and Akio K. Inoue³

¹*Subaru Telescope, National Astronomical Observatory of Japan, 650 North A'ohoku Place, Hilo, HI 96720, USA*

²*Graduate University for Advanced Studies (SOKENDAI), Osawa 2-21-1, Mitaka, Tokyo 181-8588, Japan*

³*College of General Education, Osaka Sangyo University, 3-1-1, Nakagaito, Daito, 574-8530 Osaka, Japan.*

Released 2015 Xxxxx XX

ABSTRACT

Subaru/SuprimeCam narrowband photometry of the SSA22 field reveals the presence of four Lyman continuum (LyC) candidates among a sample of 14 AGN. Two show offsets and likely have stellar LyC in nature or are foreground contaminants. The remaining two LyC candidates are Type I AGN. We argue that the average LyC escape fraction of high redshift low luminosity AGN is not likely to be unity, as often assumed in the literature. From direct measurement we obtain the average LyC-to-UV flux density ratio and ionizing emissivity for a number of AGN classes and find it at least a factor of two lower than values obtained assuming $f_{esc} = 1$. Comparing to recent Ly α forest measurements, AGNs at redshift $z \sim 3$ make up at most $\sim 12\%$ and as little as $\sim 5\%$ of the total ionizing budget. Our results suggest that AGNs are unlikely to dominate the ionization budget of the Universe at high redshifts.

Key words: cosmology: observations – diffuse radiation – galaxies: evolution – galaxies: high-redshift – intergalactic medium

1 INTRODUCTION

The intergalactic medium (IGM) is ionized and kept ionized by quasars (QSOs)/AGN and star forming (SF) galaxies. Identifying the primary population of ionizing radiation (a.k.a. Lyman Continuum, LyC) at any redshift has long been the focus of intensive studies and the situation is far from settled. The neutral hydrogen in the IGM seems to dramatically increase beyond redshift $z > 6$ (e.g. Fan et al. 2001; Becker et al. 2001; Pentericci et al. 2002), while the IGM appears to be highly ionized at $z \lesssim 6$. Some research suggests that QSOs dominate the ionization budget at redshifts $z \lesssim 3$ (e.g. Haardt & Madau 1996; Fontanot et al. 2014; Khaire & Srianand 2015; Grazian et al. 2015), others suggest that SF galaxies need to significantly contribute even at these redshifts (e.g. Faucher-Giguère et al. 2009; Glikman et al. 2011), or that the contribution of both QSOs and SF galaxies is comparable (e.g. Shull et al. 2015, $z < 2$). Observational evidence suggests that SF galaxies do not produce enough ionizing radiation at redshifts $z \leq 3$ (e.g. Grazian et al. 2015) to maintain the ionization levels, but that their ionizing emissivity substantially increases with increased redshift (e.g. Inoue et al. 2006; Becker & Bolton 2013; Duncan & Conselice 2015) and that they alone ionize the Universe at high redshifts (e.g.

Razoumov & Sommer-Larsen 2010; Alvarez et al. 2012; Bouwens et al. 2015; Duncan & Conselice 2015). The exact “turnover” redshift at which SF galaxies (including high- z low luminosity dwarfs) take over the production of ionizing photons is unclear, since their contribution seems to not be high enough to dominate the ionizing emissivity at $z = 3$ (e.g. Grazian et al. 2015) or even $z > 4$ (e.g. Cowie et al. 2009). On the other hand the luminosity function of bright QSOs suggested until recently that they are not numerous enough to dominate at $z > 6$ (e.g. Meiksin 2005; Fontanot et al. 2012, 2014). The situation may be different for faint AGN, however, for which recent research suggests a less steep decline of their number density at high redshifts. Faint AGN may in fact be numerous enough to be the main contributors to the ionizing emissivity at redshifts $z > 4$ (Giallongo et al. 2012, 2015; Madau & Haardt 2015).

Much of the literature on LyC from AGN relies on power law parameterizations of observations of quasar spectral energy distributions (SEDs). The continuum slopes can vary widely (e.g. Zheng et al. 1997; Vanden Berk et al. 2001; Telfer et al. 2002; Scott et al. 2004; Giallongo et al. 2015; Lusso et al. 2015; Cristiani et al. 2016), and often it is assumed that the average escape fraction of LyC radiation from AGN/QSOs is $\langle f_{esc} \rangle = 1$ (e.g. Giallongo et al. 2015; Madau & Haardt 2015). In this paper we take a look at a sample of AGN in the SSA22 field and analyze the detected LyC emission from Subaru/SuprimeCam narrowband data.

* Based on data collected at Subaru Telescope, which is operated by the National Astronomical Observatory of Japan

Table 1. Summary of confirmed AGN in our sample. Where available the Chandra catalog number (column L09) is indicated with the arcsec distance for coordinate cross-matching (column dist).

ID	RA	DEC	z	z Ref	L09	dist	Type	S	P[%]	Alt. name
AGN1	22:17:5.4	0:15:14.0	3.801	*	12	0.5	1	1.8	32.8	-
AGN2	22:17:5.8	0:22:25.2	3.083	*	15	1.0	2	0.7	75.6	-
AGN3 [†]	22:17:6.7	0:26:41.1	3.140	*	-	-	1	1.2	34.8	-
AGN4 [†]	22:17:9.6	0:18:0.7	3.106	Y12,L09,*	20	0.8	2	1.0	50.6	LAE J221709.6+001801
AGN5 [†]	22:17:12.7	0:28:55.6	3.110	*	-	-	1	3.8	0.0	[IKI2011] i
AGN6	22:17:16.2	0:17:44.47	3.098	S15	43	1.7	2	1.0	75.9	CXOSSA22 J221716.1+001745
AGN7	22:17:20.2	0:20:19.1	3.108	S15	57	0.2	1	7.4	0.0	LAE J221720.2+002019
AGN8	22:17:22.3	0:16:40.1	3.353	S15,VVDS	68	0.1	1	3.3	0.1	SSA 22a D013
AGN9	22:17:25.4	0:17:16.8	3.105	N13	80	0.2	2	?	?	[NSS2011] LAE 017
AGN10	22:17:35.8	0:15:59.0	3.094	S15	139	0.2	2	0.4	85.0	[GMS2005] LAB 14
AGN11 [†]	22:17:36.5	0:16:22.6	3.084	S15,VVDS	140	0.0	1	2.5	11.6	SSA 22a D012
AGN12	22:17:39.1	0:13:29.8	3.091	W05	153	0.9	2	1.1	61.7	[WYH2009] LAB 02 b
AGN13	22:17:51.3	0:20:38.4	3.460	S15	239	0.1	1	1.1	64.3	-
AGN14	22:17:59.2	0:15:29.5	3.094	S15	268	0.4	2	1.3	65.7	-

[†] - object has been detected in the *NB359* (LyC) band; * - redshift and type from spectrum in Figure A1 in the appendix; *S* - variability significance defined in Klesman & Sarajedini (2007); *P* - median probability from 10000 MC simulations for a random match to the individual light curve profiles; Type 1: broad emission lines in spectrum; Type 2: narrow emission lines; IKI2011 - Inoue et al. (2011); GMS2005 - Geach et al. (2005); NSS2011 - Nestor et al. (2011); WYH2009 - Webb et al. (2009); Y12 - Yamada et al. (2012); S15 - Saez et al. (2015); L09 - Lehmer et al. (2009); N13 - Nestor et al. (2013); W05 Wilman et al. (2005); VVDS - VIMOS VLT Deep Survey.

We present an average ionizing emissivity from direct observations, and the LyC escape fraction relative to an assumed intrinsic spectrum.

Throughout this paper we use the AB magnitude system and adopt a flat Λ CDM cosmology with $H_0 = 70 \text{ km s}^{-1} \text{ Mpc}^{-1}$, $\Omega_M = 0.3$, $\Omega_\Lambda = 0.7$.

2 SAMPLE SELECTION

We assembled a catalog of AGN from the SSA22 field by first searching among our base sample of 308 galaxies with $z > 3.06$ from Micheva et al. (2015, hereafter Paper I). With this redshift cutoff the *NB359* filter samples LyC radiation. Initially we identified 7 objects with broad emission line AGN spectral signatures, i.e. AGN of Type I. Gavignaud et al. (2008) published an updated catalog of the VIMOS VLT Deep Survey (VVDS) of broad-line (type-1) AGN with a total of 298 objects, 41 of which have redshifts $z \geq 3.06$. The only matches with our catalog are two objects already classified as broad emission line AGN from our spectra, AGN8 (SSA22a-D13) and AGN11 (SSA22a-D12). Cross-matching with the Chandra Deep Protocol Cluster Survey catalog of Xray sources in the SSA22 field (Lehmer et al. 2009) we found 12 Xray AGN among our sample. The coordinate matching tolerance for all but one object was $\leq 1.0''$ and eight of these sources were matched to better than $0.5''$. Among these Xray AGN five were already known to us as Type I AGN from their spectra while the other six were previously classified as LAEs or LBGs in our sample.

Recently, Saez et al. (2015) performed a spectroscopic survey of the SSA22 field with Keck and VLT, looking to identify new protocluster members and to complement literature studies with robust redshifts. They provide spectra of 7 Xray AGN which contain one new Xray AGN match

with our catalog. This is AGN6, with the largest coordinate matching tolerance of $1.7''$, added to our sample because the Xray emission is extended and occupies a region which contains the optical coordinates of the object in our sample (Saez, private communication). The total number of unique Type I or Xray AGN in our sample is thus 14, summarized in Table 1 and with complementary to the literature spectra in Figure A1 in the appendix. Table 1 also shows our complementary classification of the AGN in our sample, using a $\geq 1000 \text{ km s}^{-1}$ velocity width cutoff for Type I AGN, and classifying all non-Type I objects as being Type II since the quality of the spectra does not allow for a finer classification.

Among all 14 AGN four were also detected in the *NB359* narrowband data within $\leq 0.8''$ of the *R* band detection, so these constitute our initial sample of LyC AGN. Three of them are Type I (AGN3, AGN5, AGN11), and one is Type II (AGN4). The spectrum of AGN4 in the appendix shows a rest-frame velocity width of both the Ly α and the CIV lines of $\sim 670 \text{ km s}^{-1}$, and is thus clearly not Type I. Cowie et al. (2009) observe that only Xray sources with broad emission lines in their spectra have detectable ionizing flux. The ionizing radiation from AGN4 could be stellar in nature or this could be a foreground contaminant.

In Figure 1 we show the probability mass function (PMF) of the expected number of foreground contaminants using the same Monte Carlo (MC) method from Paper I which utilizes the spatial distribution of all detections in our widefield *NB359* image. The search radius used in this MC simulation is $r = 0.8''$, the largest offset we measure in the LyC AGN candidate sample. The most likely number of contaminants is zero, with a probability of full contamination of $P(\geq 4) = 0.03\%$.

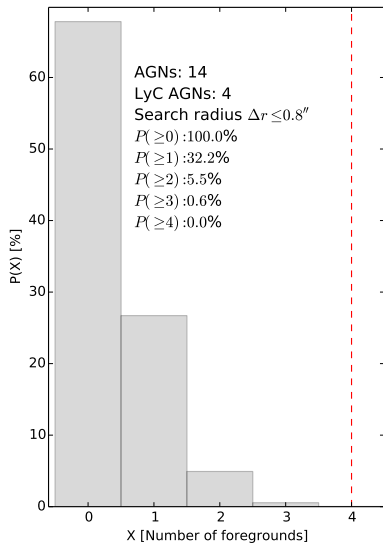


Figure 1. Probability mass function of the expected number of foreground contaminants from an MC simulation with 100000 runs. Inset text shows cumulative probabilities to obtain e.g. at least X or more contaminants. The most likely number of foreground contaminants is zero, with $P(X = 0) = 68\%$.

3 VARIABILITY

Our multiwavelength data were not taken all at the same epoch. To reliably interpret the photometry of the AGNs, and specifically their ionizing to non-ionizing flux density ratios from mixed epochs, we need to determine if they are significantly variable. Additionally, Vanzella et al. (2015) suggest that low luminosity AGN hidden in star forming galaxies could be responsible for the detected LyC emission from these galaxies. We want to check if, given the quality of our data, we can detect variability among confirmed, faint AGN. This would complement Paper I, where using the same data we tested candidates of LyC-leaking star-forming galaxies at $z \sim 3.1$, and saw no variability among them.

Xray and UV variability among AGN has been well documented in the literature in AGNs with high and intermediate-mass black holes (BH), both on short (seconds/days) and long (months/years) time scales (e.g. Ulrich et al. 1997; Netzer et al. 2003; de Vries et al. 2003, 2005; Gabel et al. 2005; Favre et al. 2005; McHardy et al. 2005; Klesman & Sarajedini 2007; Thornton et al. 2008; Miniutti et al. 2009; Ponti et al. 2012; Ludlam et al. 2015). The dominant variable component seems to be due to variability in the flux of the continuum (Parker et al. 2015), and although variability decreases towards longer wavelengths (e.g. Trèvese & Vagnetti 2002; de Vries et al. 2003), there seems to be no wavelength dependence on the variability timescale (Favre et al. 2005). Therefore, one can for example use observed UV, optical or IR long-term variability to successfully identify potential AGN candidates (e.g. Klesman & Sarajedini 2007; Trevese et al. 2008; Morokuma et al. 2008; Sarajedini et al. 2011; De Cicco et al. 2015; García-González et al. 2015). The variation and its significance are often determined by the average magnitude of all epochs, the rms around the average and

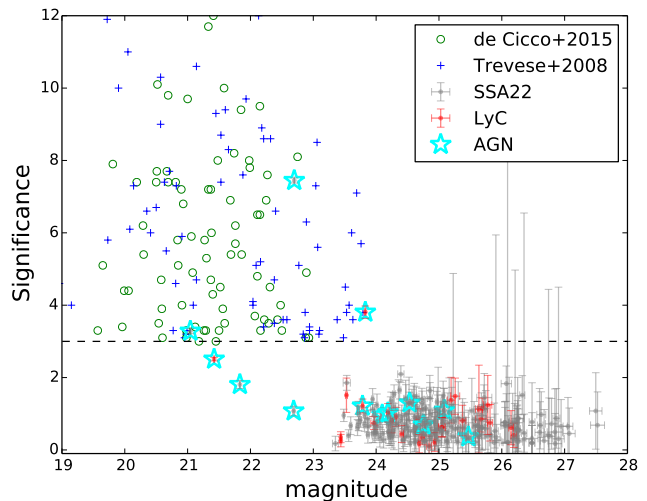


Figure 2. Variability significance versus rest-frame UV magnitude (R band) for the SSA22 sample. The Xray or spectroscopically confirmed AGN in our sample are indicated with cyan stars. The dashed line indicates the variable/non-variable separation adopting $S = \sigma/err_{\sigma} \geq 3$ as variability criterion. Variable AGNs from the VST COSMOS field (De Cicco et al. 2015) and Chandra Deep Field South (Trevese et al. 2008) are added for comparison.

an estimate of the uncertainty, from for example formal photometric errors or based on empirical estimates of the magnitude spread of non-variable objects.

We investigated the variability of our data, specifically we looked for variability among the LyC candidates in Paper I and the known AGN in our sample. We have reduced Subaru/Suprime-Cam B band data of the SSA22 field taken in the years 2002, 2003, 2007, 2008, resulting in one final frame per year. Using the NASA Extragalactic Database (NED) catalog 101 stars were identified in each frame. The year 2008 was taken as reference, the median offset in SExtractor photometry between the reference and the rest of the years was calculated, and applied to the corresponding frames. The median offsets between the stellar magnitude measurements were $\delta(2008 - 2002) = 0.27^m$, $\delta(2008 - 2003) = 0.53^m$, $\delta(2008 - 2007) = 0.31^m$. We also measured the median $FWHM$ from the stars in each frame, finding a maximum $FWHM = 1.1''$ for the year 2007.

After the zeropoints and PSFs between the 4 years were equalized we performed SExtractor photometry (MAGAUTO) on our sample of 308 LAEs, LBGs, and spectrally-confirmed AGN in Paper I, all with spectroscopically confirmed redshifts $z \geq 3.06$. There are several factors to keep in mind in our analysis. Our base sample is relatively small, especially compared to e.g. those of Trevese et al. (2008) and De Cicco et al. (2015) who have ~ 7000 , respectively ~ 18000 objects. Our individual exposures are not particularly deep, in fact we only detect 225 out of 308 objects in at least three of the four individual epochs, and < 200 in all four epochs. The bulk of our sample is several magnitudes fainter than the limits in Trevese et al. (2008) and De Cicco et al. (2015), and has significant photometric uncertainties which should be taken into account. We therefore use the

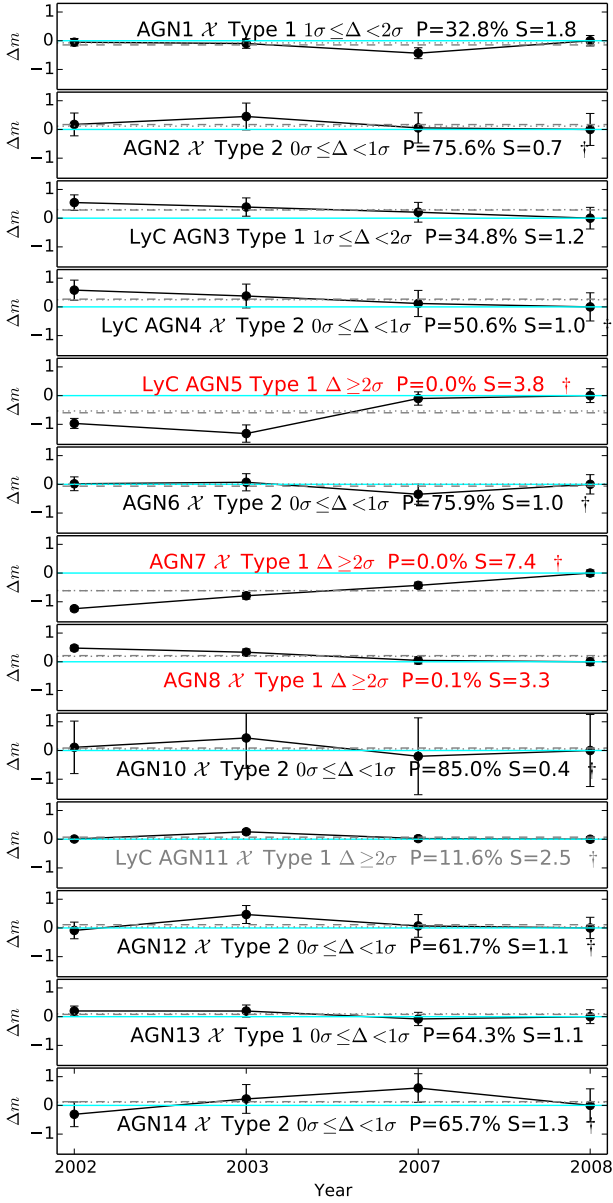


Figure 3. Light curves for all AGN in the sample. Most AGN have no detectable variability (black text), one is marginally variable (gray text), and three are significantly variable (red text). The source ID and classification (\mathcal{X} = Xray source, Type 1 or 2) are indicated for each object, as well as the variability “strength” Δ , the probability of random match to the current profile (P), and the significance (S) from the formal significance test. Protocluster association is indicated by †. Solid cyan line is at the reference year 2008 of $\Delta m = 0$. The dotted (dashed) line is the median (average) of the 4 points.

significance definition of Klesman & Sarajedini (2007), $S = \sigma / \text{err}_\sigma$, with $\text{err}_\sigma = \sqrt{\sum \sigma_m^2 / N}$, and σ_m as the formal photometric error for a magnitude measurement at a given epoch for N epochs.

We note that many studies use small apertures of fixed radius ($\sim 1''$) in an attempt to isolate the nuclei and reduce the diluting effect the host galaxy brightness has on the variability of the nucleus, while we use MAGAUTO. Our

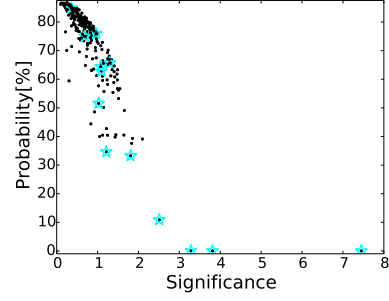


Figure 4. Random-match probability P versus variability significance S. Confirmed AGN (cyan stars) are indicated for convenience.

previous analysis (Paper I) suggested that many sources in our sample are extended and/or have several substructures. Since we do not in advance know which substructure may contain an AGN we adopted MAGAUTO as the preferred magnitude measurement.

In Figure 2 we show the significance as a function of the rest-frame UV magnitude (R band) for our sample. Only objects detected in all four epochs are considered. There are only 3 objects with significance $S \geq 3$, and hence displaying significant variability. This significance level is somewhat arbitrary since it is usually selected to keep the number of spurious detections low, as a trade off between purity and reliability. Since many of the objects of interest, i.e. confirmed AGN and LyC candidates, are below the significance limit, we also briefly investigate an alternative, more generous measure of variability in order to examine them more closely. We proceed as follows. A variability candidate is marked as “possibly variable” if its brightness deviates by $1\sigma \leq \Delta < 2\sigma$ from the 2008 reference, where $\sigma = \sqrt{\sigma_X^2 + \sigma_{2008}^2}$ is the combined photometric uncertainty, and $\Delta = (m_X - m_{2008}) / \sigma_X$, for $X = 2002, 2003, \text{ or } 2007$. A candidate is marked as “variable” if its brightness deviates by $\Delta \geq 2\sigma$ and the probability to randomly match the observed light curve is small. Sources with $\Delta < 2\sigma$ are not considered to be variability candidates.

The variability profiles (light curves) for confirmed AGNs in our sample are shown in Figure 3. We were unable to perform the variability test on the Xray AGN9 because it is below the detection limit in our B band data. To gain some idea of how significant the Δ variations are, we estimated how likely it is for a given deviation pattern to be randomly produced. The probability to obtain a random distribution of points that mimics the variability profiles we observe depends on the number of deviating points, the deviation sequence if deviating points are more than one, the amplitude of the deviation, and the size of the individual uncertainty of each measurement.

The easiest way to account for all of these factors simultaneously is to perform a Monte Carlo simulation. For each source in Figure 3 we have created an array of 3 random elements with the fourth element locked at 0 (for the reference year 2008), where each random data point was drawn from its individual Gaussian distribution with

a standard deviation equal to the uncertainty of that data point. Thus created, if all of the random profile's data points or all of their errorbars enter the region defined by $\pm 1\sigma$ of the original profile then this is considered a match to the original. For each object the total number of matches from 10000 realizations is given as the percentage probability in Table 1. This random match probability is consistent with the significance parameter S as shown in Figure 4.

In summary, three out of the 14 AGN (AGN5, AGN7, AGN8) have variability significance $S > 3$ and random match probability $P \sim 0.0\%$, all of them on the bright end with $M_R \leq -21.7$ AB. AGN11 has $S \sim 2.5$, which is fairly high, but the random match probability is not negligible, $P \sim 12\%$, and it is therefore not convincingly variable. The result of this test shows that we did not observe significant variability from low luminosity AGN ($M_R > -21.5$ AB). This implies that it is still possible for the LyC LAEs and LBGs from Paper I to be hosting low luminosity AGNs below our variability detection limit.

4 LyC AND AGN PROPERTIES

Figure 5 shows the four LyC AGNs (AGN3, AGN4, AGN5, AGN11) in our sample in the restframe UV continuum (R band, left panel), continuum-subtracted Ly α ($NB497-BV$, middle panel), and LyC emission ($NB359$, right panel). We also present the complementary images of the AGNs with non-detections in Figure B1 in the appendix. AGN3 and AGN4 are clearly morphologically different in LyC from AGN5 and AGN11, with the former two showing offsets between UV and LyC, while UV and Ly α are well aligned. If the $NB359$ detection is indeed LyC it can be coming from stars in offset starbursting regions. One could imagine a scenario in which non-stellar LyC could manifest an offset from the position of the AGN e.g. from dust scattering of the LyC from the accretion disk toward the direction of the observer, or from bound-free LyC emission from an ionized gas flow, though the latter would also scatter Ly α photons which we do not observe. The LyC-emitting offset structure in AGN3 has $\varnothing = 1.2''$ fixed aperture magnitudes $B = 26.7$, $V = 25.9$, $R = 25.7$, $i = 26.0$, $z = 25.6$, $NB497 = 25.7$, and $NB359 = 27.2$, with uncertainties ≤ 0.1 . Similarly, for AGN4 the magnitudes of the offset structure are $B = 26.6$, $V = 25.6$, $R = 25.4$, $i = 25.7$, $z = 25.6$, $NB497 = 24.2$, and $NB359 = 27.1$. All of these are well above the 3σ limiting magnitude in the corresponding filter, except the LyC detections, which are close to the limiting magnitude of $NB359(3\sigma) = 27.4^m$.

The probability to have two or more foreground contaminants in our sample is low, $P(\geq 2) = 5.5\%$, however the probability for one of them to be a contaminant is not negligible, $P(=1) = 26.7\%$. AGN3 is the most likely to be a contaminant because of its large spatial offset between LyC and UV, $\delta r = 0.8''$. In Figure C1 in the appendix we show additional available data of the two AGNs manifesting offsets. These images reveal a complicated substructure for AGN3, spatially coincident with the $NB359$ detection

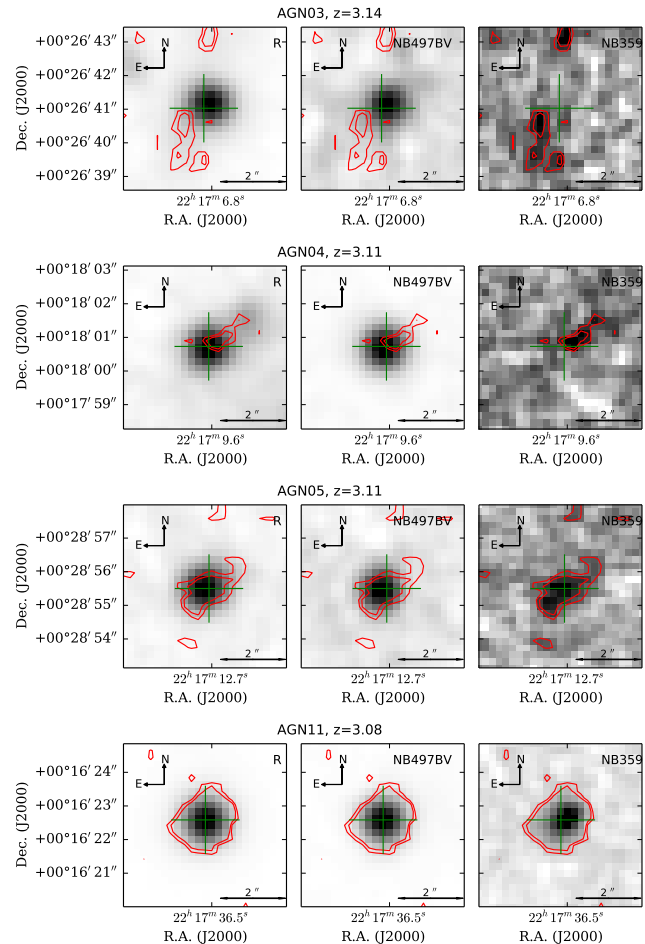


Figure 5. AGN LyC candidates. The green cross marks the location of the R band detection. The filter order is R , $NB497-BV$ (continuum-subtracted Ly α), $NB359$ (LyC). 2 and 3σ contours (red) trace the LyC detection in the $NB359$ band, and are overplotted in all other bands. AGN3 is at a redshift which places the Ly α line at the edge of the filter, and so the $NB497-BV$ image only marginally traces Ly α emission. The contrast settings in each filter are global so that brightness comparison between the AGNs is possible. The scale bar is $2''$ in all images. The color map is inverted.

and visible across all of our multiwavelength data. If the substructure is at the same redshift as AGN3, it would be an indication of an ongoing merger. For AGN4 there is an additional distinctly separate object to the North-West (NW). The LyC detection seemingly originates from the center and stretches NW towards the second object, with no visible counterpart to the LyC bridge between the two objects in the available archival Hubble Space Telescope (HST) F814W image, although the data is not very deep. If these nearby objects truly associate with the AGN host galaxies their presence may be an indication of an ongoing merger or accretion of a smaller object which may have triggered the AGN in both AGN3 and AGN4. Hereafter we refer to AGNs 3 and 4 as stellar LyC AGNs for simplicity, although their $NB359$ emission may come from contamination of foreground objects.

If both or at least one of these AGNs is indeed showing

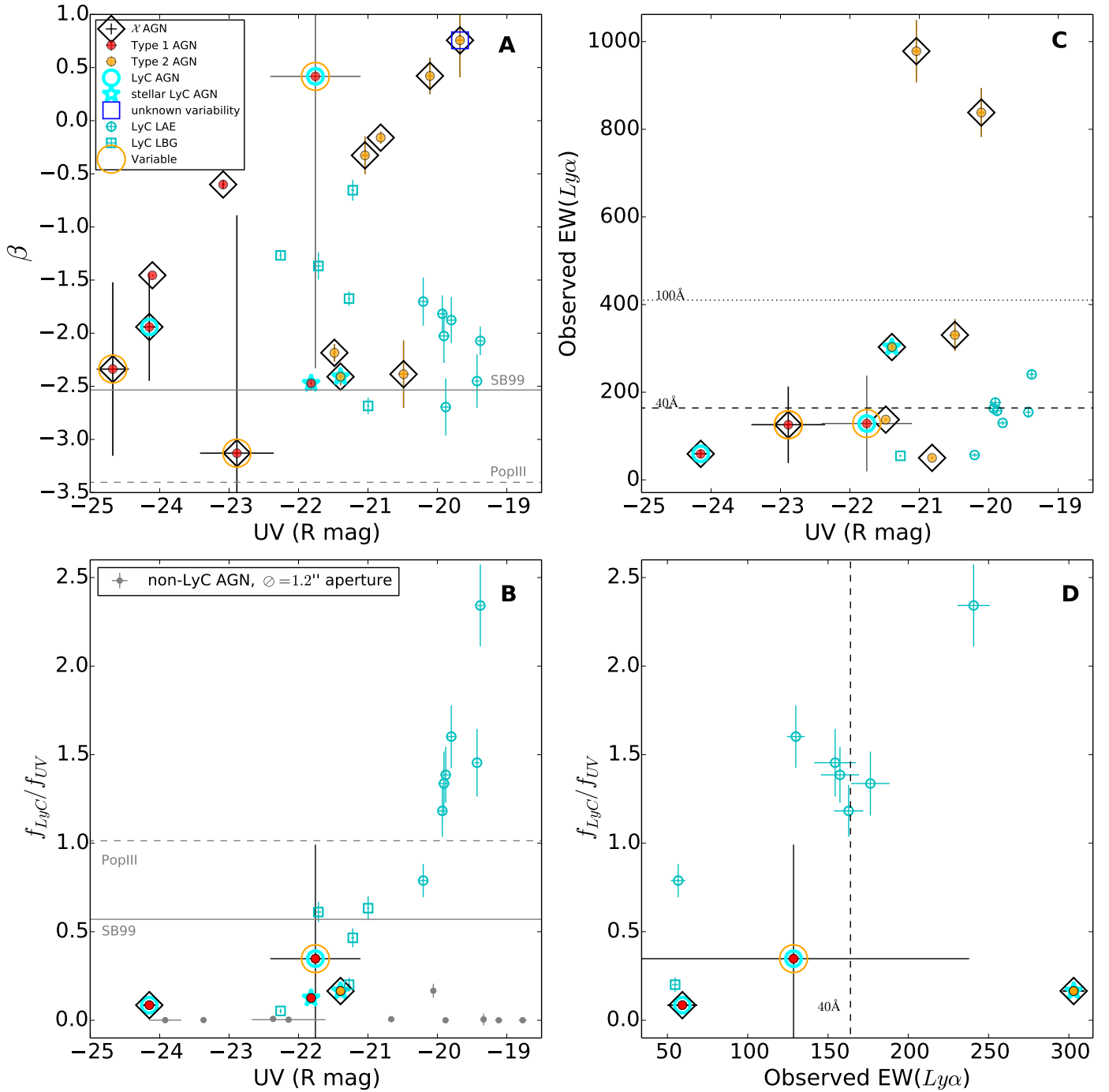


Figure 6. Comparison between LyC AGN and the non-AGN LyC candidates from Paper I. In panels A,B model predictions from STARBURST 99 (Salpeter IMF, slope $\alpha = 2.35$, metallicity $Z = 0.0004$, mass range $1-100M_{\odot}$, age 0 Myr), and PopIII (Schaerer (2003), same parameters as SB 99 except $Z = 0.0$) are shown in solid, respectively dashed lines. Gray markers in panel B are from 1.2'' aperture photometry of non-LyC AGN. Galactic extinction is applied to all measurements. LyC AGN3 is omitted from panels C,D because of its higher redshift of $z = 3.14$. AGN4 (cyan star) is deviating from the rest in panel D because of the different nature of the emission (stellar in *NB359*, coming from the AGN in all other filters). The rest-frame $EW(Ly\alpha) = 40\text{\AA}$ and 100\AA are indicated for convenience.

stellar LyC escape the corresponding detection rates of $\sim 0.14^{+0.33}_{-0.05}$ (2/14) or $\sim 0.07^{+0.24}_{-0.01}$ (1/14) are comparable to LyC LAEs and LBGs at redshift $z \sim 3.1$ (e.g. Nestor et al. 2013; Micheva et al. 2015, 6.6%-13%). The uncertainties on the detection rates are single-sided Poissonian upper and

lower limits at a 68.4% confidence level from Gehrels (1986).

The LyC detection rate for the Type I AGNs in our sample is $0.29^{+0.66}_{-0.10}$ (2/7), where we exclude stellar LyC AGN3. Compared to LyC LAEs and LBGs at the same redshift this is higher by a factor of $2.2^{+7.3}_{-1.5}$. Due to the small

Table 2. Photometry on the 14 confirmed AGN at the position of the R band detections. Omitted uncertainties are ≤ 0.1 . Uncertainties due to variability are not included.

ID	FWHM	R	$R(1.2'')$	$NB359$	$NB359(1.2'')$	$(f_{1500}/f_{900})_{obs}$	$B-V$	$NB359-R$	β (UV slope)	δr
AGN1	0.8	21.83	22.57				1.53		-1.46	
AGN2	0.8	24.75	25.52				0.69		-0.16	
AGN3	0.9	23.78	24.58	26.04 ± 0.20	28.11 ± 0.20	7.97 ± 1.42	1.18	2.25 ± 0.20	-2.47	0.8
AGN4	0.9	24.19	25.00	26.14	27.00 ± 0.12	6.06 ± 0.49	1.01	1.96	-2.41	0.5
AGN5	0.9	23.83	24.62	24.98	26.29	2.88 ± 0.19	-0.46	1.15	0.42	0.2
AGN6	0.9	24.22	25.03				0.73		-2.18	
AGN7	0.8	22.70	23.44				-0.18		-3.13	
AGN8	0.8	21.04	21.80				1.62		-2.34	
AGN9	0.9	25.91	26.79						0.76 ± 0.35	
AGN10	0.9	25.47	26.27				1.45		0.42 ± 0.17	
AGN11	0.8	21.42	22.16	24.09	24.96	11.72 ± 0.27	0.56	2.67	-1.94	0.1
AGN12	1.4	25.09	26.46				1.12		-2.39 ± 0.32	
AGN13	0.8	22.69	23.40				1.02		-0.60	
AGN14	1.2	24.53	25.69				0.87		-0.33 ± 0.18	

Note: $NB359$ samples the LyC regime at the relevant redshift of $z \geq 3.06$. FWHM(") is measured from the reference R band. Galactic extinction by Schlafly & Finkbeiner (2011) has been applied to all values. The (f_{1500}/f_{900}) column is the observed total flux density ratio of non-ionizing to ionizing radiation. β is the UV slope estimated from $V-i'$ for all AGN, except for AGN1, AGN8, AGN13 for which $R-z'$ was used. δr (") is the $R \leftrightarrow NB359$ offset in centroid position, with an astrometric uncertainty of $\sim 0.2''$.

number statistics we are unable to claim this difference is significant. Similar to Cowie et al. (2009) the detection rate among Type II AGN is 0% (0/7), where we exclude stellar LyC AGN4. Among Xray AGN the detection rate is $0.09^{+0.30}_{-0.02}$ (1/11), comparable to LyC LAEs and LBGs at the same redshift. Among protocluster members the detection rate is $0.20^{+0.46}_{-0.07}$ (2/10). We note here that regardless of which group of AGN we consider, the rate of detection is a far cry from 100%.

In the four panels of Figure 6 we examine any connection between variability, presence of Xrays, AGN type, and the properties of the LyC AGN compared to the viable LyC LAEs and LBGs candidates from Paper I (none of which are AGN), using photometry from Table 2. Confirmed and possible contaminants among LyC LAEs and LBGs are excluded from this comparison. We estimate the UV slope β from $V-i'$ for all AGN, except for the higher redshift AGN1, AGN8, and AGN13, for which we use $R-z'$ to avoid having emission lines in the filters.

Since our multiband data were not taken at the same epoch, with e.g. R in 2001 and $NB359$ in 2008, for AGN5, AGN7, AGN8, and AGN11 we add the uncertainty due to variability calculated as the dispersion of the light curves in Figure 3. This dispersion amounts to 0.65^m , 0.53^m , 0.23^m , and 0.12^m respectively. First we note that all Type II AGN are on the faint end ($\gtrsim -21.5^m$), while the majority of the Type I AGN have quasar-like luminosities ($\lesssim -23^m$). One out of two LyC AGN is variable, and both stellar LyC AGN are non-variable, suggesting that significant variability has no detectable influence on LyC leakage. There also seems to be no connection between the presence of Xrays and the LyC leakage in AGN in terms of either rest-frame UV slope or ionizing to non-ionizing flux density ratio (panels 6A and 6B). LyC LAEs and LyC LBGs have rest-frame UV slopes similar to the LyC AGN, and Ly α equivalent widths that are comparably large (panels 6A and 6C). In terms of the flux density ratio f_{LyC}/f_{UV} the LyC AGN are

comparable to LyC LBGs, and much lower than LyC LAEs (panel 6B). The ratio of the latter is notably > 1 , which is not consistent with purely stellar LyC emission and would require nebular LyC contribution (see Paper I for more details on the LyC LAEs). The LyC flux density ratio versus the $EW(Ly\alpha)$ in panel D shows that LyC AGN are consistent with the tentatively suggested correlation between Ly α and LyC in Paper I. Stellar LyC AGN4 is deviating in this figure due to the nature of the radiation being stellar in $NB359$ but coming from the AGN in all other filters. To obtain a correct (stellar) flux density ratio for this object one should subtract the AGN in the center and remeasure the photometry of the residual. We attempted to do this with GALFIT however our resolution is $FWHM \sim 1''$ which corresponds to the size of the object and the residual we obtain shows no detection above 3σ .

In panel C two AGNs show very high observed equivalent widths, AGN10 with $EW(Ly\alpha) \sim 840\text{\AA}$ and AGN14 with $EW(Ly\alpha) \sim 980\text{\AA}$. These two objects were classified as AGNs in Saez et al. (2015) due to superimposed Xray emission. We examined the SEDs of these two objects (Figure D1 in the appendix) and the imaging data in all filters. The SEDs reveal spectra redder than the typical quasar spectrum, which may indicate that they are obscured or even host-dominated. The continuum-subtracted Ly α images (Figure B1) show extended emission, which is expected for AGN10, classified as a Lyman α Blob (LAB) by Geach et al. (2005). AGN14 has not previously been identified as a LAB, however Figure B1 shows it to be even more extended than AGN10, with a clearly visible large Ly α halo.

Figure 7 shows the spectral energy distribution (SED) of the two LyC AGN, which are fairly consistent with the Vanden Berk et al. (2001) stacked spectrum at $\lambda > 1000\text{\AA}$. LyC AGN5 is strongly variable, with the multiband observations taken at different epochs. In the inset figure we add in quadrature to the formal photometry error of

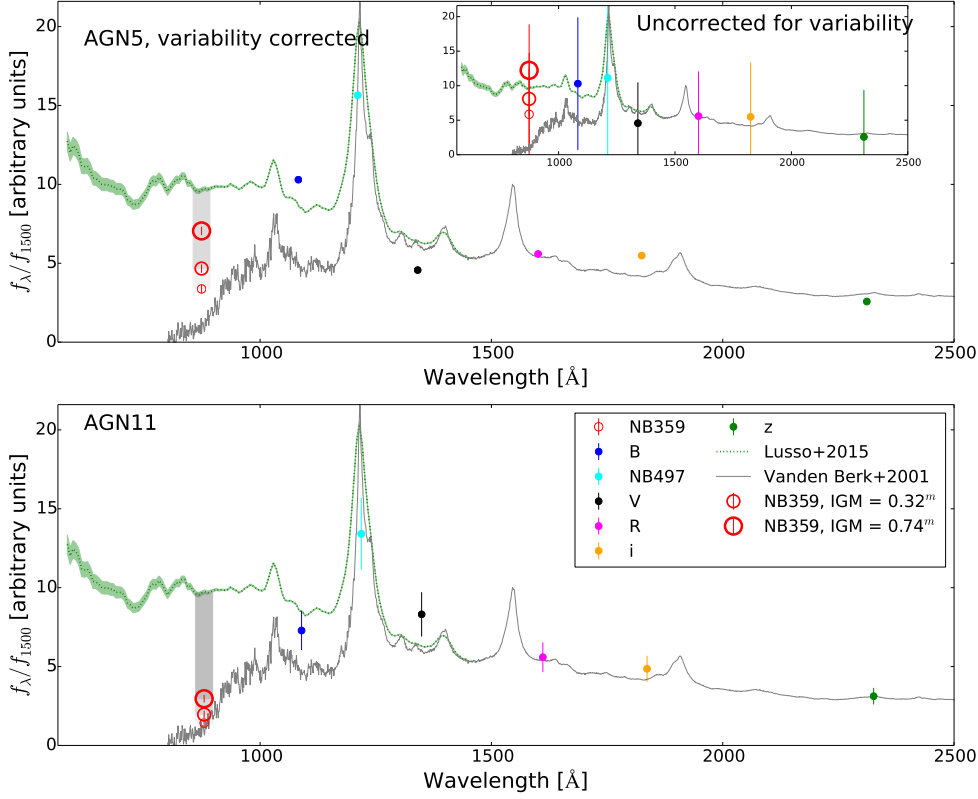


Figure 7. SEDs of the LyC-leaking AGN scaled to match the standard Vanden Berk et al. (2001) spectrum in the R band. We assume the IGM corrected stacked spectrum by Lusso et al. (2015) gives a good representation of f_{intr}^{LyC} and use it to estimate the escape fraction at the wavelength of the $NB359$ band. Gray rectangles indicate the rest-frame width of the $NB359$ band (horizontal) and the extent of f_{obs}^{LyC} to f_{intr}^{LyC} (vertical) used to obtain f_{esc} in Table 4. The inset figure for AGN5 is the uncorrected SED, with large uncertainties due to significant variability (see text for details).

each band the uncertainty due to variability, estimated from the dispersion of the light curve in Figure 3 and amounting to 0.65^m . AGN11 is marginally variable, but we add the dispersion of its light curve, which is 0.12^m . It is difficult to interpret a flux density ratio of a strongly variable object when the data are not taken in the same epoch. Without correcting the SED for variability applying a median IGM attenuation ($\tau = 0.74^m$, Inoue et al. (2014)) to the $NB359$ data point overshoots the IGM corrected spectrum, which we assume to be a good representation of the intrinsic spectrum. We therefore apply a variability correction to AGN5 by assuming the B band light curve in Figure 3 is representative of the light curves in all other filters. The correction brings all filter measurements to the level of the reference year 2008. The $NB359$ image has no correction since it was taken in the year 2008. The R , i' , and z' bands were taken in the years 2000 and 2001, which are not covered by the B band light curve. The precise correction would be the amplitude between the magnitude in 2008 and the year of observation, however since we do not have B band data in 2000, 2001 we assign the average of the light curve \bar{m} to these years and calculate their correction amplitude as $A = m(2008) - \bar{m}$. The correction resulted in brightening the R , i' , and z' fluxes by 0.60^m . The B and V bands are average stacks over the range of the light curve, so they were corrected by the same amount. The $NB497$ image was taken in 2002 so it was corrected by

the full amplitude $A = m(2008) - m(2002) = -0.97^m$.

Even with the variability correction the SED shows an excess in the B band (blue circle) compared to the Vanden Berk et al. (2001) spectrum and is instead more consistent with the intrinsic Lusso et al. (2015) spectrum. The broad OVI emission line falls well inside the B band filter (Figure A1), however from a Gaussian fit to the line we estimate that it contributes $\sim 20\%$ to the B band flux. Although the B band suffers from IGM attenuation much less than the $NB359$ (LyC) band, this may suggest an almost transparent line of sight to AGN5.

5 AVERAGE FLUX DENSITY RATIOS

The observed average flux density ratio from the AGNs in our sample is obtained through stacking and shown in Table 3. Since the sample contains Type I AGNs, which can have a broad CIV emission line falling inside of the R band filter, here we use the z' band data to measure the UV continuum. All stacks were statistically corrected for foreground contamination in a Monte Carlo (MC) simulation of 100 realizations, using the PMF of expected foreground contaminants in the same manner as in Paper I. Briefly, we make $10'' \times 10''$ cutouts of $NB359$ for each object and normalize them by the $\odot = 1.2''$ aperture flux in the

Table 3. Average flux density ratio and ionizing emissivity ϵ_{LyC} [10^{24} erg s $^{-1}$ Hz $^{-1}$ Mpc $^{-3}$] at $z \sim 3.1$ from direct measurement for two magnitude ranges $(-18.0, -28.0)$ and $(-20.0, -28.0)$. The z' band samples the UV continuum. All values have been statistically corrected for foreground contamination. Non-detections are given as 3σ upper limits. The uncertainties in the $\langle z' \rangle$ and $\langle V - i' \rangle$ columns are < 0.03 , < 0.05 respectively. The errors on ϵ_{LyC} include luminosity function uncertainties. N is the number of stacked objects.

CASE A						
Full sample, no variability correction						
max sample size = 13						
Stack	$\langle f_{LyC}/f_{UV} \rangle$	$\langle z' \rangle$	$\langle V - i' \rangle$	$\epsilon_{LyC}(-18.0, -28.0)$	$\epsilon_{LyC}(-20.0, -28.0)$	N
all	< 0.045	23.50	0.05	< 0.481	< 0.423	= 13
LyC	0.109 ± 0.012	23.01	0.10	1.164 ± 0.132	1.025 ± 0.117	≤ 3
TypeI	0.051 ± 0.006	22.75	0.04	0.546 ± 0.068	0.481 ± 0.060	≤ 7
TypeI \cap Xray	< 0.033	22.61	0.01	< 0.352	< 0.310	≤ 5
Xray	< 0.057	23.45	0.04	< 0.606	< 0.533	≤ 11
noLyC \cap TypeI	< 0.009	22.59	0.01	< 0.099	< 0.087	= 3
noLyC \cap Xray	< 0.059	23.62	0.05	< 0.634	< 0.559	= 9
CASE B						
stellar LyC excluded, no variability correction						
max sample size = 11						
Stack	$\langle f_{LyC}/f_{UV} \rangle$	$\langle z' \rangle$	$\langle V - i' \rangle$	$\epsilon_{LyC}(-18.0, -28.0)$	$\epsilon_{LyC}(-20.0, -28.0)$	
all	< 0.055	23.37	0.07	< 0.586	< 0.516	= 11
LyC	0.139 ± 0.015	22.84	0.20	1.489 ± 0.160	1.311 ± 0.141	≤ 2
TypeI	0.049 ± 0.006	22.61	0.04	0.527 ± 0.069	0.464 ± 0.061	≤ 5
TypeI \cap Xray	0.016 ± 0.003	22.43	0.02	0.169 ± 0.033	0.149 ± 0.029	≤ 4
Xray	< 0.058	23.36	0.04	< 0.618	< 0.545	≤ 10
noLyC \cap TypeI	< 0.013	22.59	0.01	< 0.138	< 0.121	= 3
noLyC \cap Xray	< 0.069	23.62	0.05	< 0.740	< 0.652	= 9
CASE C						
stellar LyC excluded, variability corrected						
max sample size = 11						
Stack	$\langle f_{LyC}/f_{UV} \rangle$	$\langle z' \rangle$	$\langle V - i' \rangle$	$\epsilon_{LyC}(-18.0, -28.0)$	$\epsilon_{LyC}(-20.0, -28.0)$	
all	< 0.053	23.62	0.05	< 0.570	< 0.502	= 11
LyC	0.092 ± 0.009	22.60	0.18	0.981 ± 0.094	0.864 ± 0.083	≤ 2
TypeI	0.035 ± 0.004	22.57	0.03	0.372 ± 0.042	0.327 ± 0.037	≤ 5
TypeI \cap Xray	0.015 ± 0.002	22.45	-0.01	0.166 ± 0.026	0.146 ± 0.023	≤ 4
Xray	< 0.060	23.39	0.01	< 0.641	< 0.564	≤ 10
noLyC \cap TypeI	< 0.009	23.39	-0.04	< 0.099	< 0.087	= 3
noLyC \cap Xray	< 0.065	23.39	0.00	< 0.698	< 0.615	= 9
CASE D						
stellar LyC and variable AGN excluded						
max sample size = 8						
Stack	$\langle f_{LyC}/f_{UV} \rangle$	$\langle z' \rangle$	$\langle V - i' \rangle$	$\epsilon_{LyC}(-18.0, -28.0)$	$\epsilon_{LyC}(-20.0, -28.0)$	
all	< 0.077	23.66	0.18	< 0.827	< 0.728	= 8
LyC(AGN11)	0.062 ± 0.003	21.94	0.03	0.661 ± 0.029	0.582 ± 0.026	≤ 1
TypeI	0.031 ± 0.003	22.41	0.21	0.334 ± 0.033	0.294 ± 0.029	≤ 2
TypeI \cap Xray	0.031 ± 0.004	22.42	0.22	0.327 ± 0.039	0.288 ± 0.034	≤ 2
Xray	< 0.078	23.80	0.24	< 0.833	< 0.734	≤ 8
noLyC \cap TypeI	< 0.019	22.88	0.58	< 0.205	< 0.181	= 1
noLyC \cap Xray	< 0.084	24.46	0.50	< 0.894	< 0.787	= 7
CASE E						
Type I AGN at $z \sim 3.1$						
max sample size = 4						
Stack	$\langle f_{LyC}/f_{UV} \rangle$	$\langle z' \rangle$	$\langle V - i' \rangle$	$\epsilon_{LyC}(-18.0, -28.0)$	$\epsilon_{LyC}(-20.0, -28.0)$	
TypeI	0.060 ± 0.009	22.96	-0.04	0.646 ± 0.099	0.569 ± 0.087	≤ 4

z' band. In each MC run we draw a random number of contaminants n_{cont} based on the PMF of expected number of foreground contaminants, with a separate PMF obtained for each sample size. If the total number of candidates is n and the number of non-detections in NB359 N , we

make a stack with $N + n - n_{cont}$ and measure the flux density ratio inside a $\odot = 1.2''$ aperture. If $n_{cont} \geq n$ then only N number of images are stacked. If the stack consists only of LyC candidates the flux density ratio is set to zero for that MC run. The result is the average value of 100

such realizations. We estimate the uncertainty of the flux density ratio in the following way. For the i th object in the j th realization we sample 100 random sky positions in the *NB359* band, normalize each by object i 's z' band flux, and measure the aperture sums. The uncertainty per object, $\sigma_{i,j}$, is the standard deviation of these 100 aperture sums. The uncertainty per average stack in MC run j is then $\sigma_{stack,j} = \sqrt{\sum \sigma_{i,j}^2 / N}$, $i = 1 \dots N$ where $N = N + n - n_{cont}$ is the total number of objects stacked. The final uncertainty of the flux density ratio we present in Table 3 is the average of 100 MC runs.

We considered five cases, shown in Table 3. In all cases we exclude AGN1 because due to its higher redshift ($z = 3.8$) the z' band covers a different rest-frame wavelength range than the rest of the sample. Case A takes the sample of 13 AGNs, including the two stellar LyC AGNs. Case B excludes the two stellar LyC AGNs and AGN1. Case C is like B but applies a variability correction to the photometry of the three variable AGNs. Case D is like B but considers only non-variable AGNs. Case E considers only a stack of the four Type I AGN at redshifts $3.084 \leq z \leq 3.140$. Cases have subgroups consisting of all objects, only LyC candidates, all Type I AGNs, all Xray AGNs, all Type I AGNs with Xray, all Type I AGNs with non-detections in *NB359*, and all Xray AGNs with non-detections in *NB359*. For case D the subgroup of only LyC candidates contains just one object, AGN11. Table 3 also shows $\langle z' \rangle$ and $\langle V - i' \rangle$ which sample the UV continuum and slope.

The variability corrections for Case C were obtained for all three variables as described in Section 4, namely we assign an average magnitude \bar{m}_B to the missing 2001 data point from the B band light curve, measure the amplitude $A = m_B(2008) - \bar{m}_B$ and use it to correct the $V i' z'$ fluxes. The corrections brighten these fluxes by 0.60^m and 0.62^m for AGN5 and AGN7, respectively, and dim the fluxes by 0.21^m for AGN8.

6 IONIZING EMISSIVITY

The literature often assumes an average escape fraction of unity and a double power law spectrum to estimate the ionizing emissivity of high- z AGNs. Since we have direct measurements of the LyC-to-UV flux density ratios from two AGN in our sample, we could instead compute the observed ionizing emissivity, and compare it to results which assume a unity escape fraction. We will refer to the emissivity obtained from direct LyC measurement as ϵ_{LyC} , the emissivity from assuming a double power law spectrum with $f_{esc} = 1$ as ϵ_{912} , and the emissivity inferred from Ly α forest observations as $\epsilon_{912}^{L\alpha F}$. Throughout this section the emissivity is in comoving units of 10^{24} erg s $^{-1}$ Hz $^{-1}$ Mpc $^{-3}$. To calculate ϵ_{LyC} we use the quasar luminosity function from Masters et al. (2012) at redshift $z = 3.2$. This is described by a double power-law function with parameters $\phi_* = 2.65(\pm 2.22) \cdot 10^{-7}$ Mpc $^{-3}$ mag $^{-1}$, $\alpha = -2.98 \pm 0.21$, $\beta = -1.73 \pm 0.11$, and $M_* = -25.54 \pm 0.68$ at $\lambda = 1450\text{\AA}$. Since we are sampling the UV continuum at the position of the z' band ($\lambda_{eff} = 2317\text{\AA}$), we scale M_*^{1450} to M_*^{2317} using the Lusso et al. (2015) spec-

trum. The non-ionizing emissivity is then given by

$$\epsilon_{UV} = \int \phi(L_{2317,z}) L_{2317} dL_{2317} \quad (1)$$

where ϕ is the luminosity function, L_{2317} is the non-ionizing UV continuum luminosity. For the magnitude range of the integration $(-18, -28)$ and $(-20, -28)$, the resulting non-ionizing emissivity is $\epsilon_{UV,24} = 5,111$, respectively $4,501$, where the subscript 24 means 10^{24} erg s $^{-1}$ Hz $^{-1}$ Mpc $^{-3}$. The ionizing emissivity can be calculated as $\epsilon_{LyC} = \mathcal{R} \epsilon_{UV}$, where \mathcal{R} is the flux density ratio $f_{LyC} / f_{UV} e^{\tau_{IGM}}$ and may be luminosity dependent as seen in Figure 6B. For the observed average flux density ratio we use the direct detections or the 3σ upper limits in Table 3 for the four cases we considered. The IGM attenuation is assumed to be $\tau_{IGM} = 0.74^m$, which is the median of the MC simulation in the new IGM transmission model in Inoue & Iwata (2008) but with an updated IGM absorbers statistics described in Inoue et al. (2014). Table 3 shows the resulting ionizing emissivities for all cases and subgroups. The error budget in ϵ_{LyC} includes the flux density ratio and luminosity function uncertainties, added in quadrature.

Many ϵ_{LyC} reported in the literature assume a double power law and $f_{esc} = 1$. It is immediately obvious from our data that the average escape fraction is most likely not unity. To further illustrate this we calculate the ionizing emissivity assuming a double power law spectrum following Giallongo et al. (2015), with $f_\lambda \propto \lambda^\alpha$ with $\alpha = 1.57$ for $\lambda \leq 1200\text{\AA}$, and $f_\lambda \propto \lambda^\beta$ with $\beta = 0.44$ for $\lambda > 1200\text{\AA}$. It is equally interesting to compare our ϵ_{LyC} from direct measurements to the value obtained using the Lusso et al. (2015) IGM corrected spectrum, which has steeper values of $\alpha = 1.70$ for $\lambda \leq 912\text{\AA}$ and $\beta = 0.61$ for $\lambda > 912\text{\AA}$. These two equations are

$$\epsilon_{912} = \int \phi(L_{2317,z}) L_{2317} \left(\frac{912}{1200} \right)^{1.57} \left(\frac{1200}{2317} \right)^{0.44} dL_{2317} \quad (2)$$

$$\epsilon_{912} = \int \phi(L_{2317,z}) L_{2317} \left(\frac{912}{2317} \right)^{0.61} dL_{2317} \quad (3)$$

With Eq. 2 (Giallongo) the ionizing emissivity becomes $\epsilon_{912,24} = 2.487$ and 2.190 , respectively for the magnitude ranges $(-18, -28)$ and $(-20, -28)$. With Eq. 3 (Lusso) the values are $\epsilon_{912,24} = 2.894$ and 2.549 . The largest value for $\epsilon_{LyC,24}$ in Table 3 is obtained for the subgroup of only LyC AGN candidates (Case C, variability corrected), $\epsilon_{LyC,24} = 0.981 \pm 0.094$ for $(-18, -28)$. This group is not representative of all AGN and may be biased towards high escape fractions. Even so, the ionizing emissivity from direct measurement $\epsilon_{LyC,24}$ is lower than the $f_{esc} = 1$ case $\epsilon_{912,24}$ values by a factor of ~ 2.5 . For the more representative Type I subgroup it is a factor of ~ 6.7 lower. The discrepancy increases for Case D (non-variable AGN). Even if we only look at Type I AGNs strictly at $z \sim 3.1$ (Case E), $\epsilon_{LyC,24}$ is a factor of ~ 3.8 lower than $\epsilon_{912,24}$. We note that $\epsilon_{LyC,24}$ for Case B is larger than for all other cases, being only a factor of ~ 1.7 lower than $\epsilon_{912,24}$. However, we remind the reader that this case contains no variability correction and the LyC and UV continua are sampled at different time epochs, which makes their ratio

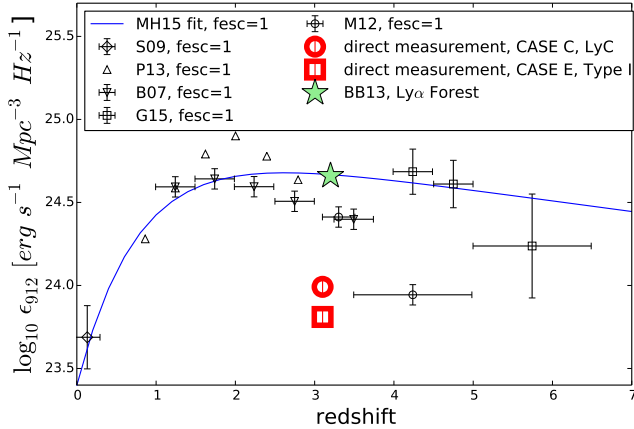


Figure 8. Ionizing emissivity vs. redshift, reproduced from Madau & Haardt (2015, MH15). The Becker & Bolton (2013, BB13) emissivity at $z = 3.2$ inferred from Ly α forest observations in quasar spectra is shown with a green star symbol. Our direct measurement of ϵ_{LyC} (thick red markers) is given for the largest but biased value (Case B, LyC subgroup), and for Type I AGN between $3.084 \leq z \leq 3.140$ (Case E). Literature results (open black markers) compiled by MH15, all inferred from quasar luminosity functions assuming $f_{esc} = 1$, are shown from Schulze et al. (2009, S09), Palanque-Delabrouille et al. (2013, P13), Bongiorno et al. (2007, B07), Giallongo et al. (2015, G15), Masters et al. (2012, M12). The line is the MH15 fit through the $f_{esc} = 1$ literature data. All literature data has been re-scaled to M_{\star}^{2317} .

hard to interpret.

Our direct measurement $\epsilon_{LyC,24}$ is sampled at $\lambda \sim 876\text{\AA}$ instead of at the Lyman edge 912\AA , but the ratios $\epsilon_{912}/\epsilon_{876}$ for both double power laws are very close to unity, namely $\epsilon_{912}/\epsilon_{876} = 1.08$ for Eq. 2 and $\epsilon_{912}/\epsilon_{876} = 1.04$ for Eq. 3. The observed difference between direct measurement of LyC and assuming a power law can therefore not be explained by the wavelength region at which LyC is being sampled.

In Figure 8 we reproduce the emissivity vs. redshift plot of Madau & Haardt (2015), who compile quasar luminosity function data from the literature, convert the integrated optical emissivity using the new Lusso et al. (2015) stacked spectrum, assume average $f_{esc} = 1$, and infer the ionizing emissivity for different redshifts. We overplot our emissivity ϵ_{LyC} from direct detections for the largest value in Table 3 (Case C, LyC subgroup) and for the Type I AGNs at redshift $z \sim 3.1$ (Case E). Both fall clearly far beneath the $f_{esc} = 1$ emissivities. Becker & Bolton (2013) infer the ionizing emissivity at $z = 3.2$ from observations of the Ly α forest in composite quasar spectra. They obtain $\epsilon_{912,24}^{Ly\alpha F} = 8.147$. Our ϵ_{LyC} from direct measurement fall obviously short of sustaining such levels and further appear to not dominate the ionization budget at this redshift since they only make up at most 12% (Case C, LyC subgroup) and as little as $\sim 5\%$ (Case E) of $\epsilon_{912,24}^{Ly\alpha F}$. This may imply that faint AGN, even if significantly more numerous at high redshifts than previously thought (Giallongo et al. 2015), may not contribute enough to f_{esc} to ionize the Universe at

Table 4. LyC escape fraction of the four Type I AGN at redshift $z \sim 3.1$ relative to the Lusso et al. (2015) IGM corrected intrinsic spectrum. Escape fractions at the restframe effective wavelength (λ_{eff}^{LyC}) are stated for a transparent line of sight ($\tau = 0$), a “minimum” IGM attenuation ($\tau = 0.32^m$), and a median IGM attenuation ($\tau = 0.74^m$). A variability correction of -0.60^m , -0.62^m was applied to the R band flux for AGN5, AGN7. 3σ upper limits are shown for the non-detections AGN3 and AGN7.

ID	λ_{eff}^{LyC} [Å]	$f_{esc}^{\tau=0}$	$f_{esc}^{\tau=0.32}$	$f_{esc}^{\tau=0.74}$	$err(f_{esc})$
AGN3	867.1	< 0.008	< 0.011	< 0.016	
AGN5	873.5	0.35	0.48	0.73	0.30
AGN7	873.9	< 0.003	< 0.004	< 0.007	
AGN11	879.0	0.15	0.20	0.31	0.27

high redshifts.

Finally, we note that we performed the same calculations with the luminosity function of $z \sim 4$ optically-selected QSOs by Glikman et al. (2011). The former parameterization has larger uncertainties than Masters et al. (2012), and the resulting non-ionizing emissivity $\epsilon_{UV,24}$ is lower, albeit roughly consistent within the uncertainties, with the values we obtain from Masters. This change of luminosity function does not alter our conclusions.

7 LyC ESCAPE FRACTION FROM AGN

Lusso et al. (2015) stack 53 luminous quasars at $z \simeq 2.4$ and apply an average IGM transmission correction. Their corrected spectrum thus represents an intrinsic spectrum of redshift $z \simeq 2.4$ quasars. Quasar spectra appear to be similar in a wide range of redshifts (Vanden Berk et al. 2001, $0.044 \leq z \leq 4.789$), so we assume there is no redshift evolution of the quasar continuum from $z \sim 2.4$ to our redshift of $z \sim 3.1$. The Lusso stack is dominated by non-Xray sources (43 out of 53), while our sample is dominated by Xray AGN (12 out of 14). However, the difference between sources with and without strong Xray emission seems to be in the lines, not in the continuum (e.g. Green 1998), and the comparison of our sample to Lusso’s is therefore fairly reasonable. We further assume that the average bright quasar has a similar spectrum to the average faint/moderately bright AGN.

Under these assumptions we can use the Lusso IGM corrected spectrum as a reasonable approximation of the intrinsic spectrum of AGNs at redshift ~ 3.1 . We can then calculate the escape fraction of LyC relative to this intrinsic spectrum, $f_{esc}(LyC) = f_{obs}^{LyC} e^{\tau_{IGM}} / f_{intr}^{LyC}$. We present three resulting fractions, assuming a transparent line of sight to the AGN (no IGM correction), and assuming a “minimum” ($\tau = 0.32^m$) and median ($\tau = 0.74^m$) IGM attenuation for the observed *NB359* (LyC) flux. The “minimum” IGM correction is obtained from the same transmission model as the median (Inoue & Iwata 2008; Inoue et al. 2014) as the smallest 0.15% value of the MC simulation. We note that the IGM transmission model used by Lusso et al. (2015, their Figure 3) on redshift $z = 2.4$ objects results in transmission $T_{\lambda} \sim 0.62$ at the LyC filter’s rest-frame

wavelengths λ of our objects. For the same redshift and wavelength the Inoue et al. (2014) IGM model gives a very similar transmission of $T_\lambda = 0.66$.

The f_{esc} values of all four Type I AGNs at redshift $z \sim 3.1$ (AGN3, AGN5, AGN7, AGN11) are shown in Table 4, with upper limits for AGN3 and AGN7. Here we treat AGN3 as a non-detection in LyC due to the unclear nature of the offset emission in the *NB359* filter. Since f_{obs}^{LyC} is obtained from the *NB359* band with width 150\AA , the f_{intr}^{LyC} is taken as the average over a $150\text{\AA}/(1+z)$ wavelength bin, centered at the restframe effective wavelength of the *NB359* band for each AGN. This is illustrated in Figure 7 with gray rectangles at the *NB359* position. The indicated errors of f_{esc} in Table 4 are the photometric uncertainty in the *NB359* measurement added in quadrature to the average uncertainty in the IGM corrected Lusso spectrum in the relevant wavelength interval. This interval is marked as gray rectangles in Fig. 7. For AGN5 and AGN7 we present f_{esc} from a variability-corrected SED, with formal errors.

The suggested escape fractions for all cases are smaller than unity, consistent with the low emissivities we obtain in Figure 8.

8 DISCUSSION

The AGN in our sample fall short of matching ionizing emissivities inferred from assuming average $f_{esc} = 1$. They are fainter than high- z quasars however, so it is still possible that bright quasars have escape fractions $f_{esc} = 100\%$. If we were to only look at the three brightest AGN in Figure 6A, which have quasar-like luminosities ($M < -25.0$ in Fig 6B), the LyC detection rate is only 33% (1 out of 3). It is possible that the other two bright AGN (AGN8 at $M_R = -24.99$, and AGN1 at $M_R = -24.35$) are completely obscured by the intervening IGM. Using the brightest AGN as an example (AGN8 at $z \sim 3.4$), we calculate the probability to dim a source of a given apparent magnitude m_{LyC} down to the 2σ limiting magnitude of $NB359(2\sigma) = 27.5^m$, i.e. below our detection threshold. If we assume that AGN8 will have similar LyC brightness as the brightest LyC AGN (AGN11, $M_R = -24.48$, $z \sim 3.1$), then $m_{LyC} = 24.1$. To dim such an object to $NB359(2\sigma)$ we need at least a 3.5 magnitude obscuration. According to the IGM Monte Carlo simulation from Inoue & Iwata (2008) and Inoue et al. (2014) the probability for full LyC obscuration is then $P(\geq 3.5) = 50.6\%$. We can instead assume that the LyC emission is given by the intrinsic Lusso et al. (2015) IGM corrected spectrum, which has a $f_{LyC}/f_{UV} \sim 2.0$. Thus, the apparent LyC magnitude of this object should be $m_{LyC} = 20.3$, and a dimming by 7.3^m is required, with probability for full obscuration $P(\geq 7.3) = 40.8\%$. For AGN1 at $z \sim 3.8$ the corresponding probabilities are $P(\geq 3.5) = 80.2\%$ and $P(\geq 7.3) = 70.7\%$.

All of these probabilities are significant and we cannot reject $f_{esc} = 100\%$ for each individual object. To calculate the probability of simultaneous obscuration of two or more objects we assume that the lines of sight and therefore the probabilities are independent. The correlation in the trans-

verse Ly α forest flux in quasar absorption spectra has been measured by e.g. D’Odorico et al. (2006) and Coppolani et al. (2006), and is significant at the 3σ level up to angular separations of $\lesssim 6$ comoving Mpc. The minimum angular separation among the five Type I AGNs in our sample which are also non-detections in the LyC filter is $221''$ (~ 7 comoving Mpc at $z \sim 3.1$). The assumption of independent lines of sight therefore seems reasonable.

The probabilities for both AGN1 and AGN8 to be fully obscured simultaneously are then $P = 0.41 * 0.71 \sim 29\%$ or $P = 0.80 * 0.71 \sim 57\%$, which are lower but still significant. For an object at $z \sim 3.1$, the probability for full obscuration assuming the Lusso spectrum is only $P(\geq 7.3) = 10.3\%$. The probability to fully obscure the two Type I AGNs which are members of the proto-cluster and show non-detections in LyC (AGN3, AGN7, $z \sim 3.1$) is then $P(\geq 7.3) = 0.1^2 = 1.1\%$, which seems very low. To obscure all five Type I AGNs (AGN1, AGN3, AGN7, AGN8, AGN13, $z \sim 3.1-3.46$) the probability is $P(\geq 7.3) = 0.71 * 0.10 * 0.41 * 0.10 * 0.49 \sim 0.1\%$, which is negligible. It therefore seems unlikely that IGM obscuration could account for the low detection rate we observe, suggesting that the average escape fraction from moderately bright/faint AGN is not unity.

One should further consider that there is a non-zero probability to have at least two foreground contaminants in our sample. If the detections we observe in the *NB359* filter come from low- z galaxies then this would only strengthen our conclusion that the observed detection rates are not easily explained with IGM obscuration, and therefore the data seem inconsistent with $\langle f_{esc} \rangle = 1$.

Recently, Cristiani et al. (2016) stacked 1669 bright quasars from the SDSS BOSS survey and find an average $f_{esc} = 0.7$. Their sample is however at a higher redshift and a brighter magnitude range. Their faintest quasars are $\sim 2^m$ brighter than our brightest AGNs.

9 CONCLUSIONS

We present Subaru/SuprimeCam *BVRi'z'*, Ly α , LyC broadband and narrowband photometry for a sample of 14 spectroscopically confirmed $z > 3.08$ AGN from the SSA22 field, as well as six spectra to complement the available literature. Four AGN are detected in the LyC filter. Two LyC detections show offsets and are likely stellar in nature. For the remaining two AGN the LyC is spatially coincident with the UV continuum and Ly α emission, with no measureable offsets between UV and Ly α to LyC within our astrometry uncertainty. The statistical probability to have at least three foreground contaminants in this sample is 0.6%.

If the nature of the LyC detection in the two AGNs showing a spatial offset between LyC and UV is indeed stellar (probability for contamination $P(\geq 2) = 5.5\%$), then the detection rate of stellar LyC from AGN seems fairly high - at least $\sim 0.07_{-0.01}^{+0.24}$ (1/14) or even $\sim 0.14_{-0.05}^{+0.33}$ (2/14). This is comparable to star forming LBGs and LAEs at the

same redshift. The detection rate among Type I AGNs is $0.29^{+0.66}_{-0.10}$ (2/7), which is higher than star forming galaxies, although not significantly so within the uncertainties.

Through stacking we obtain average flux density ratios and ionizing emissivity for e.g. LyC, Type I, Xray, and $z = 3.1$ subgroups, statistically corrected for foreground contamination. The largest emissivity we obtain accounts for at most 12% and as little as 5% of the ionization budget predicted by Ly α forest observations in quasar spectra at the same redshift. Our direct measurement of the ionizing emissivity of Type I AGNs is on average a factor of ~ 7 lower than the emissivity obtained from assuming a double power law with $f_{esc} = 1$. Our sample indicates that the average f_{esc} does not seem to be unity. It is possible for individual AGNs to be fully obscured by the intervening IGM, however the probability that e.g. all five out of the seven Type I AGNs in the sample are fully obscured is negligible, $P = 0.1\%$. This may suggest that faint AGN, even if more numerous than previously thought, are not sufficient to completely dominate the ionization budget of the Universe at high redshifts.

Examining the properties of the AGN we find that three are significantly variable and 12 are Xray sources. The small numbers prevent us from discerning any possible connection between variability and Xray emission to LyC escape.

ACKNOWLEDGMENTS

GM and II are supported by JSPS KAKENHI Grant number: 24244018. GM acknowledges support by the Swedish Research Council (Vetenskapsrådet). AKI is supported by JSPS KAKENHI Grant number: 26287034.

A part of this research has made use of the NASA/ IPAC Infrared Science Archive, which is operated by the Jet Propulsion Laboratory, California Institute of Technology, under contract with NASA.

We extend a warm thank you to Yuichi Matsuda, Katsuki Kousai, Elisabeta Lusso, Cristian Saez, and Alice Shapley for providing us with their spectra, and with some clarifications on their work and helpful advice. We also thank Andrea Grazian for useful suggestions and comments on this work.

APPENDIX A: SPECTRA OF THE AGN SAMPLE

The majority of the spectra of the presented sample can be found in the catalogs of Saez et al. (2015), Matsuda et al. (2012), Wilman et al. (2005), Nestor et al. (2013) or the VVDS online database. The missing spectra are for AGN1, AGN2, AGN3, AGN4, and AGN5 which we show here for completion.

APPENDIX B: MOSAICS OF NON-DETECTIONS IN LyC

Here we show the complementary images of the LyC non-detections. For high- z AGN the $NB497-BV$ images do not

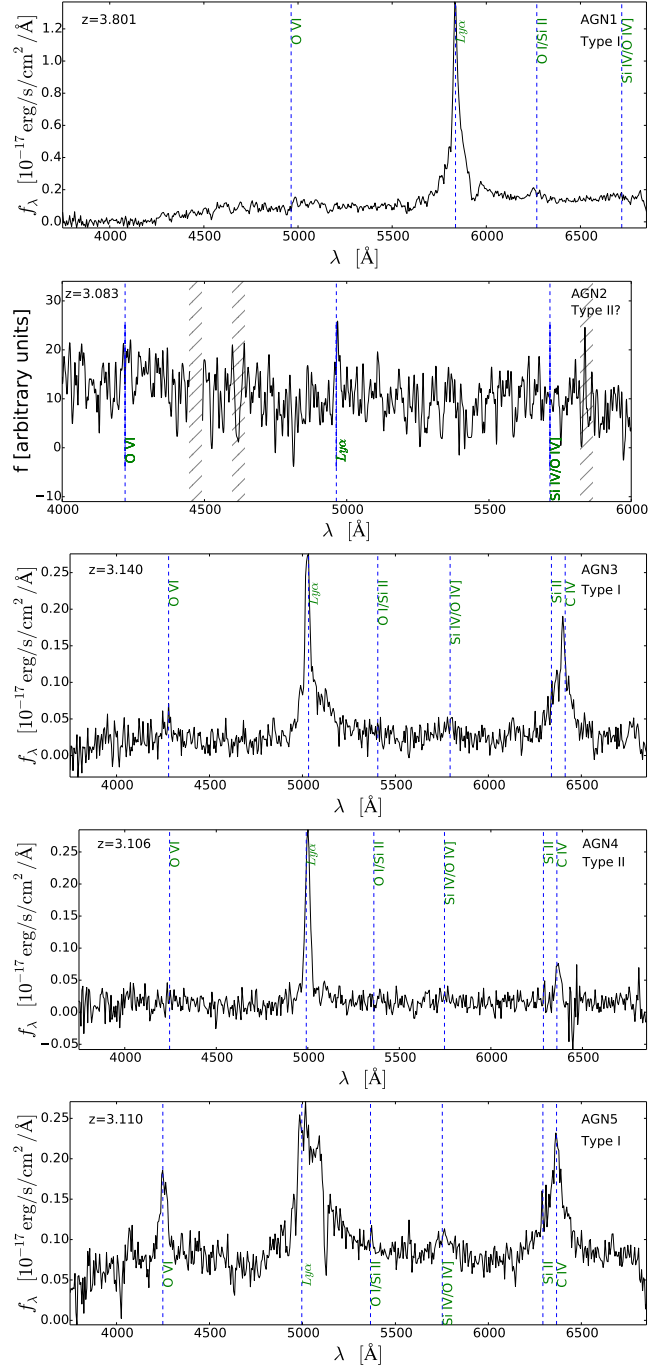


Figure A1. Complementary spectra of the AGN sample. Data are from DEIMOS 2004 (AGN2), VIMOS 2006 (AGN1, AGN4), VIMOS 2008 (AGN3, AGN5). These spectra are used solely to demonstrate the redshift and classification of these AGN.

trace continuum subtracted Ly α , so we show instead the $NB497$ images which simply sample the UV continuum.

APPENDIX C: EXTRA IMAGES OF AGN3 AND AGN4

To investigate the nature of the offset LyC detection in these AGNs we present a selection of additional images.

APPENDIX D: SEDS OF LABS AGN10 AND AGN14

These two AGNs are also Lyman α Blobs and show extreme observed $EW(Ly\alpha)$ and extended $Ly\alpha$ emission. Their SEDs in Figure D1 reveal a spectrum much redder than the typical quasar spectrum.

APPENDIX E: PHOTOMETRY CATALOG OF THE AGN SAMPLE

This work comes with an online catalog of $BVRi'z'$ broad-band photometry, narrowband $NB359$ (LyC at $z > 3.06$) and $NB497$ ($Ly\alpha$ at $3.06 < z < 3.127$) for all 14 AGN in our sample. The catalog contains AB magnitude measurements from asymptotic growth curve measurements (total mag) and from a $\phi = 1.2''$ fixed aperture photometry.

REFERENCES

- Alvarez M. A., Finlator K., Trenti M., 2012, *ApJ*, 759, L38
 Becker G. D., Bolton J. S., 2013, *MNRAS*, 436, 1023
 Becker R. H., Fan X., White R. L., et. al. 2001, *AJ*, 122, 2850
 Bongiorno A., Zamorani G., Gavignaud I., et. al. 2007, *A&A*, 472, 443
 Bouwens R. J., Illingworth G. D., Oesch P. A., et. al. 2015, *ApJ*, 811, 140
 Coppolani F., Petitjean P., Stoehr F., Rollinde E., Pichon C., Colombi S., Haehnelt M. G., Carswell B., Teyssier R., 2006, *MNRAS*, 370, 1804
 Cowie L. L., Barger A. J., Trouille L., 2009, *ApJ*, 692, 1476
 Cristiani S., Serrano L. M., Fontanot F., Koothrapalli R. R., Vanzella E., Monaco P., 2016, *ArXiv e-prints*
 De Cicco D., Paolillo M., Covone G., et al. 2015, *A&A*, 574, A112
 de Vries W. H., Becker R. H., White R. L., 2003, *AJ*, 126, 1217
 de Vries W. H., Becker R. H., White R. L., et al. 2005, *AJ*, 129, 615
 D'Odorico V., Viel M., Saitta F., Cristiani S., Bianchi S., Boyle B., Lopez S., Maza J., Outram P., 2006, *MNRAS*, 372, 1333
 Duncan K., Conselice C. J., 2015, *MNRAS*, 451, 2030
 Fan X., Narayanan V. K., Lupton R. H., Strauss M. A., et. al. 2001, *AJ*, 122, 2833
 Faucher-Giguère C.-A., Lidz A., Zaldarriaga M., et. al. 2009, *ApJ*, 703, 1416
 Favre P., Courvoisier T. J.-L., Paltani S., 2005, *A&A*, 443, 451
 Fontanot F., Cristiani S., Pfrommer C., et. al. 2014, *MNRAS*, 438, 2097
 Fontanot F., Cristiani S., Vanzella E., 2012, *MNRAS*, 425, 1413
 Gabel J. R., Kraemer S. B., Crenshaw D. M., et al. 2005, *ApJ*, 631, 741
 García-González J., Alonso-Herrero A., Pérez-González P. G., et al. 2015, *MNRAS*, 446, 3199
 Gavignaud I., Wisotzki L., Bongiorno A., et al. 2008, *A&A*, 492, 637
 Geach J. E., Matsuda Y., Smail I., et. al. 2005, *MNRAS*, 363, 1398
 Gehrels N., 1986, *ApJ*, 303, 336
 Giallongo E., Grazian A., Fiore F., et. al. 2015, *A&A*, 578, A83
 Giallongo E., Menci N., Fiore F., et. al. 2012, *ApJ*, 755, 124
 Glikman E., Djorgovski S. G., Stern D., et. al. 2011, *ApJ*, 728, L26
 Grazian A., Giallongo E., Gerbasi R., et. al. 2015, *ArXiv e-prints*
 Green P. J., 1998, *ApJ*, 498, 170
 Haardt F., Madau P., 1996, *ApJ*, 461, 20
 Inoue A. K., Iwata I., 2008, *MNRAS*, 387, 1681
 Inoue A. K., Iwata I., Deharveng J.-M., 2006, *MNRAS*, 371, L1
 Inoue A. K., Kousai K., Iwata I., Matsuda Y., et. al. 2011, *MNRAS*, 411, 2336
 Inoue A. K., Shimizu I., Iwata I., Tanaka M., 2014, *MNRAS*, 442, 1805
 Khaire V., Srianand R., 2015, *MNRAS*, 451, L30
 Klesman A., Sarajedini V., 2007, *ApJ*, 665, 225
 Lehmer B. D., Alexander D. M., Chapman S. C., et. al. 2009, *MNRAS*, 400, 299
 Ludlam R. M., Cackett E. M., Gültekin K., et al. 2015, *MNRAS*, 447, 2112
 Lusso E., Worseck G., Hennawi J. F., Prochaska J. X., Vignali C., Stern J., O'Meara J. M., 2015, *MNRAS*, 449, 4204
 Madau P., Haardt F., 2015, *ApJ*, 813, L8
 Masters D., Capak P., Salvato M., Civano F., Mobasher B., Siana B., Hasinger G., Impey C. D., Nagao T., Trump J. R., Ikeda H., Elvis M., Scoville N., 2012, *ApJ*, 755, 169
 Matsuda Y., Yamada T., Hayashino T., et. al. 2012, *MNRAS*, 425, 878
 McHardy I. M., Gunn K. F., Uttley P., et al. 2005, *MNRAS*, 359, 1469
 Meiksin A., 2005, *MNRAS*, 356, 596
 Micheva G., Iwata I., Inoue A. K., Matsuda Y., Yamada T., Hayashino T., 2015, *ArXiv e-prints*
 Miniutti G., Ponti G., Greene J. E., et al. 2009, *MNRAS*, 394, 443
 Morokuma T., Doi M., Yasuda N., et al. 2008, *ApJ*, 676, 163
 Nestor D. B., Shapley A. E., Kornei K. A., et. al. 2013, *ApJ*, 765, 47
 Nestor D. B., Shapley A. E., Steidel C. C., Siana B., 2011, *ApJ*, 736, 18
 Netzer H., Kaspi S., Behar E., et al. 2003, *ApJ*, 599, 933
 Palanque-Delabrouille N., Magneville C., Yèche C., et al. 2013, *A&A*, 551, A29
 Parker M. L., Fabian A. C., Matt G., et al. 2015, *MNRAS*, 447, 72
 Pentericci L., Fan X., Rix H.-W., et. al. 2002, *AJ*, 123, 2151
 Ponti G., Papadakis I., Bianchi S., et al. 2012, *A&A*, 542, A83
 Prochaska J. X., Hennawi J. F., Lee K.-G., Cantalupo S., Bovy J., Djorgovski S. G., Ellison S. L., Lau M. W., Martin C. L., Myers A., Rubin K. H. R., Simcoe R. A., 2013, *ApJ*, 776, 136
 Razoumov A. O., Sommer-Larsen J., 2010, *ApJ*, 710, 1239

Saez C., Lehmer B. D., Bauer F. E., et al. 2015, MNRAS, 450, 2615
 Sarajedini V. L., Koo D. C., Klesman A. J., et al. 2011, ApJ, 731, 97
 Schaerer D., 2003, A&A, 397, 527
 Schlafly E. F., Finkbeiner D. P., 2011, ApJ, 737, 103
 Schulze A., Wisotzki L., Husemann B., 2009, A&A, 507, 781
 Scott J. E., Kriss G. A., Brotherton M., Green R. F., Hutchings J., Shull J. M., Zheng W., 2004, ApJ, 615, 135
 Shull J. M., Moloney J., Danforth C. W., et al. 2015, ApJ, 811, 3
 Steidel C. C., Erb D. K., Shapley A. E., Pettini M., Reddy N., Bogosavljević M., Rudie G. C., Rakic O., 2010, ApJ, 717, 289
 Telfer R. C., Zheng W., Kriss G. A., Davidsen A. F., 2002, ApJ, 565, 773
 Thornton C. E., Barth A. J., Ho L. C., et al. 2008, ApJ, 686, 892
 Trevese D., Boutsia K., Vagnetti F., et al. 2008, A&A, 488, 73
 Trèvese D., Vagnetti F., 2002, ApJ, 564, 624
 Ulrich M.-H., Maraschi L., Urry C. M., 1997, ARA&A, 35, 445
 Vanden Berk D. E., Richards G. T., Bauer A., et al. 2001, AJ, 122, 549
 Vanzella E., de Barros S., Castellano M., et al. 2015, A&A, 576, A116
 Webb T. M. A., Yamada T., Huang J.-S., et al. 2009, ApJ, 692, 1561
 Wilman R. J., Gerssen J., Bower R. G., Morris S. L., Bacon R., de Zeeuw P. T., Davies R. L., 2005, Nature, 436, 227
 Yamada T., Nakamura Y., Matsuda Y., et al. 2012, AJ, 143, 79
 Zheng W., Kriss G. A., Telfer R. C., Grimes J. P., Davidsen A. F., 1997, ApJ, 475, 469

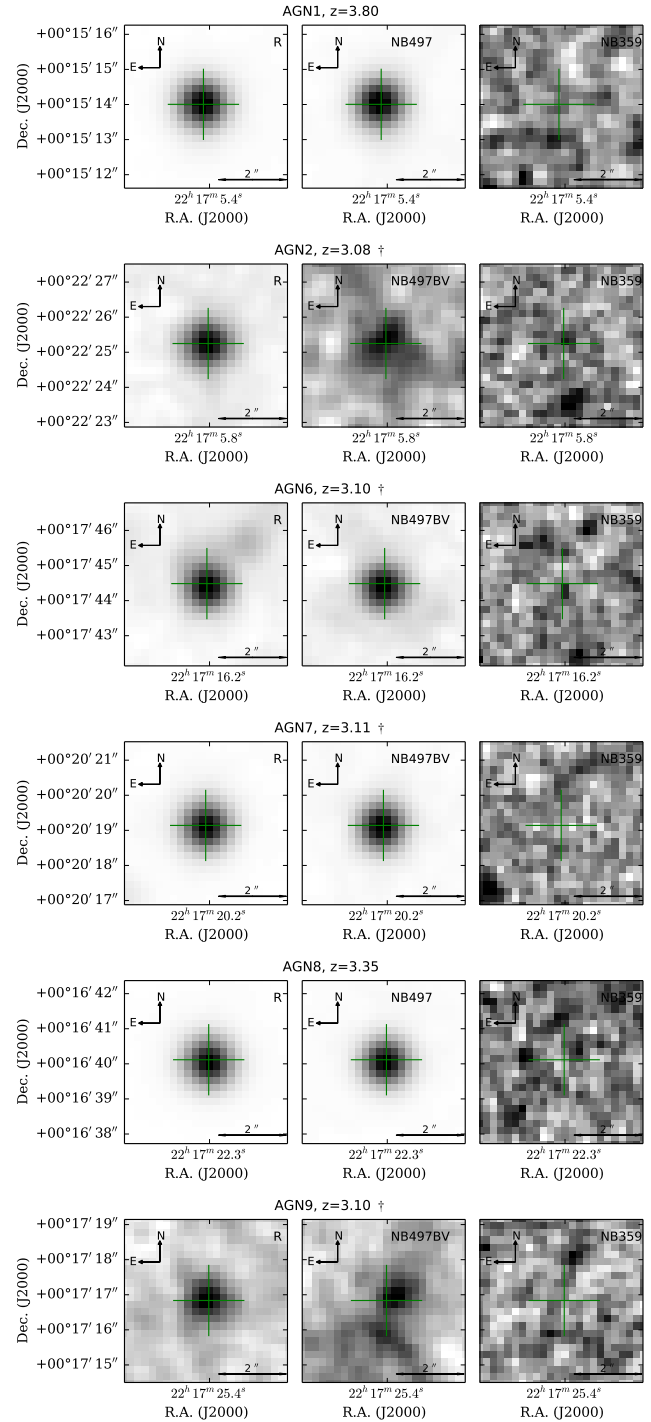


Figure B1. Complementary images for all non-detections in LyC. The *NB497–BV* image (middle column) shows continuum subtracted Ly α emission for redshifts $3.06 \leq z \leq 3.12$, indicated with a dagger. For higher- z AGN we show the *NB497* image instead. The *NB359* image (right column) shows LyC. The contrast and intensity settings are the same as in Figure 5.

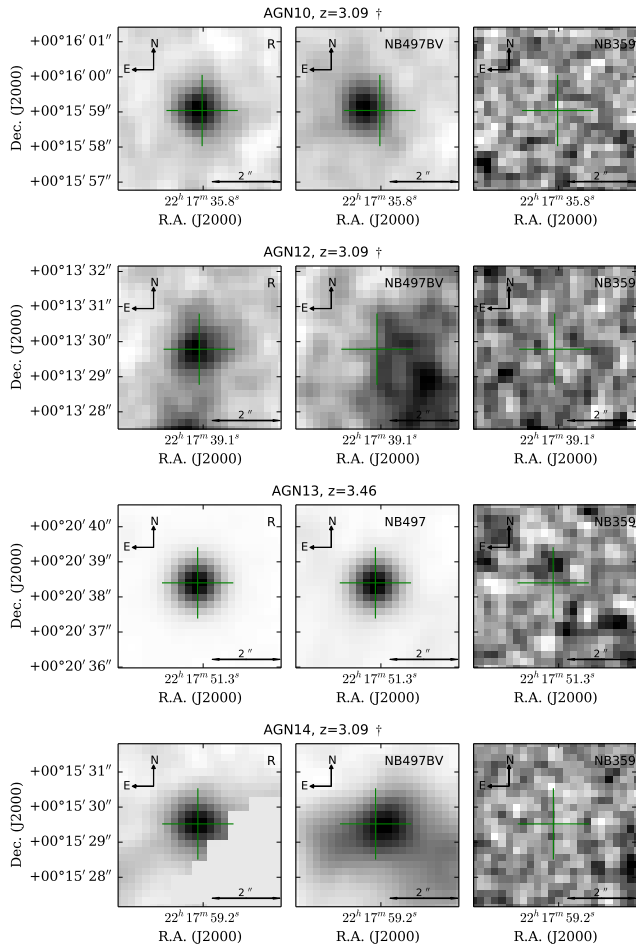


Figure B1 – *continued*

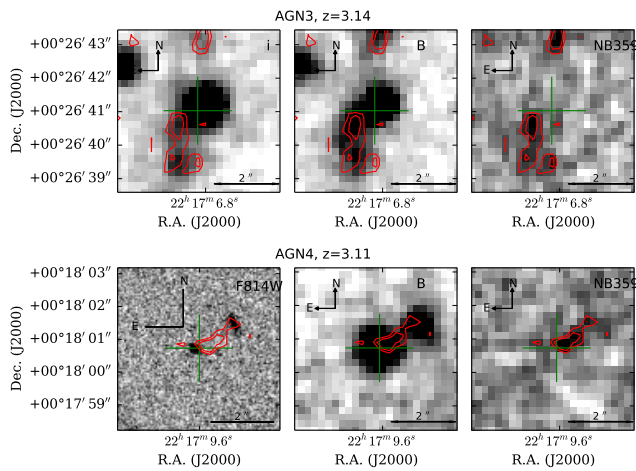


Figure C1. Additional images for stellar LyC AGN3 (*i'*, *B*) and LyC AGN4 (HST *F814W*, *B*).

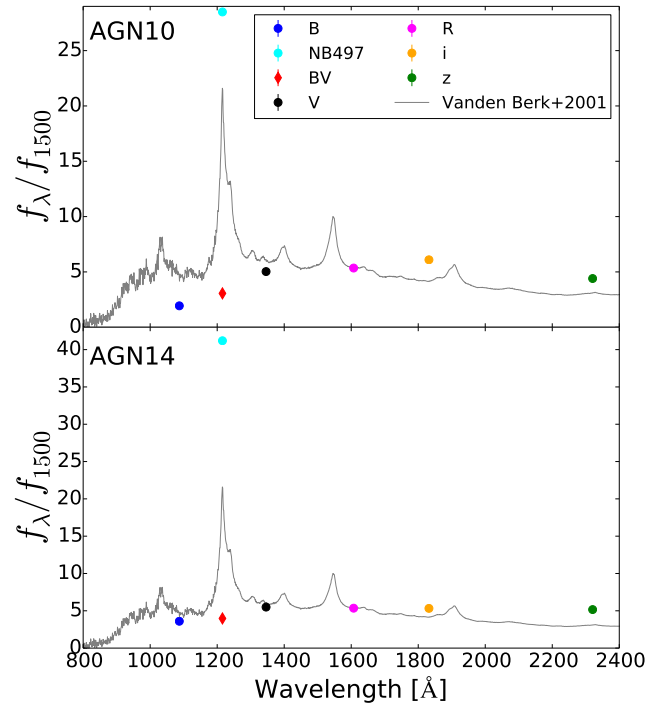


Figure D1. SEDs of LABs AGN10 and AGN14 showing their red spectrum and extreme Ly α .